Directed Network Mapping Approach to Rotor Localization in Atrial Fibrillation Simulation

Muhamed Vila[1], Sara Rocher[2], Massimo W Rivolta[1], Javier Saiz[2] and Roberto Sassi[1]

Abstract— Catheter ablation for atrial fibrillation (AF) is one of the most commonly performed electrophysiology procedures. Despite significant advances in our understanding of AF mechanisms in the last years, ablation outcomes remain suboptimal for many patients, particularly those with persistent or long-standing AF. A possible reason is that ablation techniques mainly focus on anatomic, rather than patient-specific functional targets for ablation. The identification of such ablation targets remains challenging. The purpose of this study is to investigate a novel approach based on directed networks, which allow the automatic detection of important arrhythmia mechanisms, that can be convenient for guiding the ablation strategy. The networks are generated by processing unipolar electrograms (EGMs) collected by the catheters positioned at the different regions of the atria. Network vertices represent the locations of the recordings and edges are determined using cross-covariance time-delay estimation method. The algorithm identifies rotational activity, spreading from vertex to vertex creating a cycle. This work is a simulation study and it uses a highly detailed computational 3D model of human atria in which sustained rotor activation of the atria was achieved. Virtual electrodes were placed on the endocardial surface, and EGMs were calculated at each of these electrodes. The propagation of the electric wave fronts in the atrial myocardium during AF is very complex, so in order to properly capture wave propagation patterns, we split EGMs into multiple short time frames. Then, a specific network for each of these time frames was generated, and the cycles repeating in consecutive networks point us to the stable rotor's location. The respective atrial voltage map served as reference. By detecting a cycle between the same 3 nodes in 19 out of 58 networks, where 10 of these networks were in consecutive time frames, a stable rotor was successfully located.

I. INTRODUCTION

Catheter ablation has been recommended as a first-line treatment for atrial fibrillation (AF) termination. Ablation procedures have been primarily focused on isolating the pulmonary veins (PVs), often complemented by left atrial posterior wall isolation [1]. Although these procedures, based on anatomical targets, are often successful in terminating paroxysmal AF, the ability to terminate persistent AF remains disappointing [2]. As an alternative, ablation approaches, guided by activation maps obtained from electroanatomical mapping systems, try to localize and target AF drivers (such as focal activation or stable rotors), but significant concerns

remain about their accuracy [3]. Using phase analysis of endocardial atrial signals recorded with a basket catheter, in [4] authors introduced Focal Impulse and Rotor Modulation (FIRM), a technology capable of identifying localized rotors as sources of AF. However, a debate over the phase mapping technique is ongoing. It was shown that phase mapping easily generates false positives [5], especially due to local activation time (LAT) variations on the signals and large inter-electrode distances. In order to further improve the efficacy of catheter ablation for AF, new tools for the assessment of cardiac excitation patterns are needed to help us determine the underlying mechanisms and to identify the appropriate ablation targets.

Inspired by a recent work in which directed networks were used to characterize the excitation of the human heart [6], in this paper we investigated a directed network based approach to represent electrical activity in the atria during AF. The networks are obtained by processing electrograms and are able to characterize some important features of the excitation pattern that can help in guiding the ablation strategy.

II. METHODS

A. Geometrical and electrical atrial model

A realistic 3D model of the human atria [7] that included heterogeneity at cell, tissue and organ scale was used. The model includes different anatomical regions with their respective fiber orientation. This computational finite element model is composed of linear hexahedral elements with a regular spatial resolution of 300 μm. See [7] for additional details about the model.

The cellular electrical activity is modelled by the Courtemanche-Ramírez-Nattel (CRN) ionic model [8]. In order to reproduce transmembrane potential (V_m) of experimentally observed heterogeneity in action potential (AP) morphologies and duration in the different atrial regions, the conductances of three specific ionic currents (*i.e.*, I_{to}, I_{CaL} and I_{Kr}) were adjusted for 8 different regions in both atria [7], [9]. This procedure generated nine different cellular models and the AP duration variation among regions was similar to experimental observations [10].

The electrical propagation was solved by the mono-domain formalism using the operator splitting numerical scheme (constant time step of 0.01 ms) with the ELVIRA solver [11]. The simulations were run on a computing node with sixty-four 16-core Intel® Xeon® Gold 6130 clocked at 2.10 GHz.
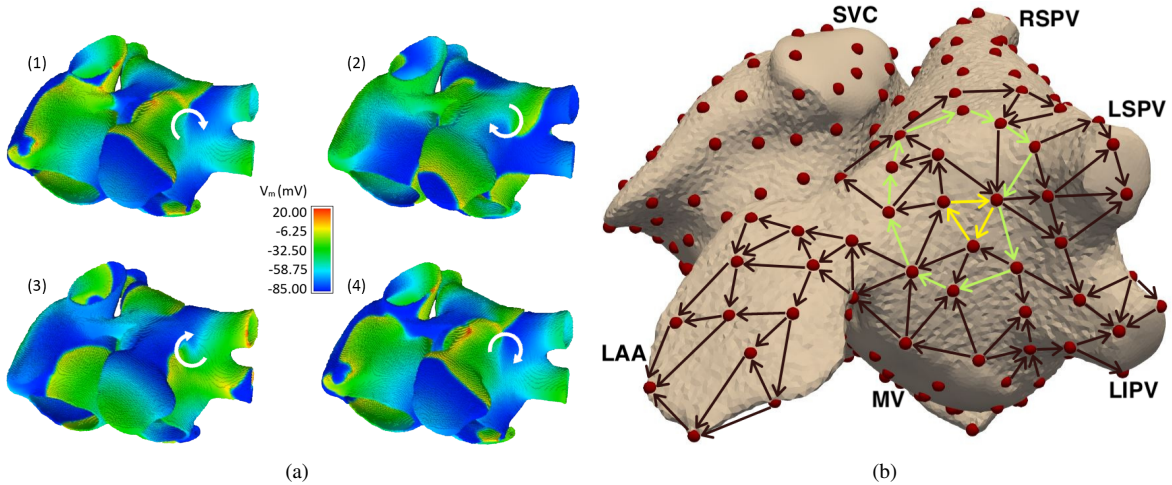
Fig. 1: Rotor detection in the network. Panel (a) shows 4 snapshots of the simulated V_m in the 3D atrial model at $t = 4200$ ms (1), $t = 4233$ ms (2), $t = 4266$ ms (3) and $t = 4299$ ms (4). It is possible to observe a rotational activity in the left atrium, right in between the PVs and the left atrial appendage (white arrow). Panel (b) shows a portion of the network mapped in the rotor's region, generated for time interval from 4100 ms to 4400 ms. Red dots represent EGMs and arrows represent their connections. The smallest cycle, made of 3 nodes and indicated in yellow, detects the center of the rotor. The bigger cycle, indicated in light green, shows the larger area of influence of the rotor. LSPV=Left Superior PV, RSPV=Right Superior PV, LIPV=Left Inferior PV, MV=Mitral Valve, LAA=Left Atrial Appendage, SVC=Superior Vena Cava.

B. The simulated fibrillation pattern

A sustained high frequency train of stimuli (100 ms cycle length) was applied in the right atrium, close to the coronary sinus. This led to a complex fibrillatory pattern with the presence of reentrant drivers. More specifically, we were able to observe two rotors, one in the right atrium, very close to the superior vena cava, and the other in the left atrium, right in between the left PVs and the left atrial appendage. Figure 1a shows the simulation snapshots that display direction of wave propagation and the rotor in the left atrium. The simulation was run for a total of 6 seconds.

C. EGM calculation and preprocessing

Unipolar electrograms (EGMs) were computed on the endocardial surface as extracellular potentials, with a temporal resolution of 1 ms, in a whole atrial-torso model [7]. We computed 400 EGMs, equidistant from each other: half of them in the left and the other half in the right atrium (with 6.5 mm average distance between two EGMs). Spatial distribution of EGMs is visible on Figure 1b.

Next, EGMs were preprocessed with bandpass filtering (third-order Butterworth filter with cutoffs of 40–250 Hz), rectification, and lowpass filtering (third-order Butterworth filter with a 20 Hz cutoff) [12]. The preprocessing resulted in a signal proportional to the amplitude of high-frequency components (*i.e.*, atrial beats), enhancing the periodicity of the signal.

D. Directed network mapping

To create the directed networks, first, the Delaunay triangulation was applied to determine the neighbours of each of the 400 virtual electrodes placed in the atria. After all the neighbors were set, each of the EGMs were divided into 300 ms time segments, using a sliding window of 100 ms. This resulted in total of 58 different time segments for our 6 s simulation. For each of these time segments, a specific network was generated.

In order to determine the existence and the direction of the connections between all the pairs of neighbors, we used a cross-covariance-based time-delay estimation method. Suppose EGM A and EGM B form a pair of neighbors. We simply allowed a directed link from EGM A to EGM B if the estimated delay from A to B (determined by the argument of the maximum of the cross-covariance) was positive and if the conduction velocity (Euclidean distance between the two EGMs divided by the delay) was in between a minimal and maximal conduction velocity values. These values were set at minimal 0.1 mm/ms and maximal 2 mm/ms, according to physiological limits. The rationale for the use of the cross-covariance to estimate the delays was that the identification of the LATs during AF is challenging.

E. Rotor detection in the network

Once the networks were created, any type of rotational activity could be found by detecting cycles in the networks. A cycle is defined as a non-empty directed trail in which the first and last node coincide.

In order to find the center of the rotor, we looked for the smallest possible cycles in the networks, *i.e.* cycles that contain only three nodes. After finding all the smallest cycles in all the networks, we counted how many times the same cycle repeated throughout different networks (that represent different time frames). The cycles repeating in consecutive networks pointed us to the location of a stable rotor.
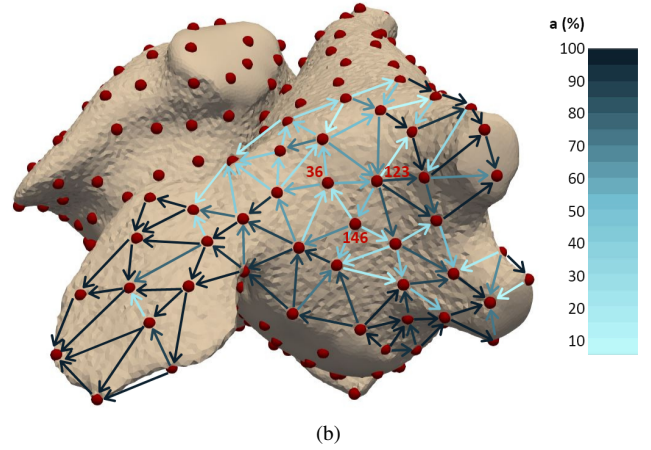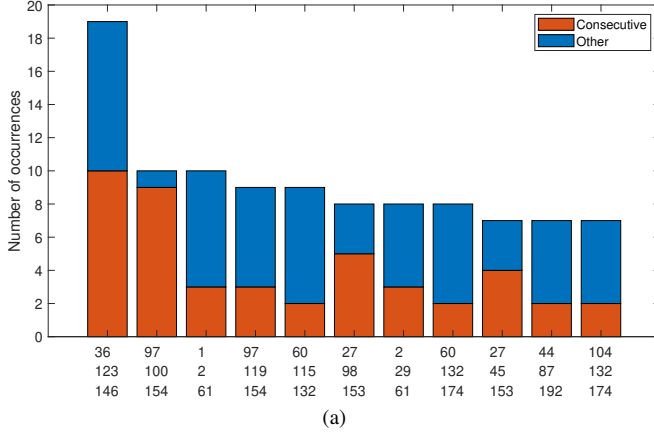
(a)

(b)

Fig. 2: Panel (a) shows graphs that contain cycles with exactly three nodes that occurred in 7 or more networks. IDs of the nodes are contained on horizontal axis, and number of occurrences is on vertical axis. Red color indicates the longest sequence of consecutive occurrences. Panel (b) shows a portion of the result obtained by network averaging formula, focusing on the region where the rotor is located. The cycle with the largest number of occurrences (36,123,146) is visible. Please, refer to Figure 1b for the name of the anatomical regions.

Another application of directed networks is network averaging to describe the cardiac excitation pattern (*e.g.*, [6]). In this study, for each node, the average connection was computed using the following formula:

$$a_{A \to B} = \frac{\sum_{n=1}^{N} c_{AB}^n - \sum_{n=1}^{N} c_{BA}^n}{N} \cdot 100\%,$$

where $c_{AB}^n = 1$ if a connection from node A to node B exist in the n-th network (and vice versa for c_{BA}^n), and $N = 58$ is the total number of networks. Considering that $a_{A \to B} = -a_{B \to A}$ is always true, for the averaged network we only show arrows where $a_{A \to B}$ has a value greater than zero. The value of $a_{A \to B}$ represents the strength of connectivity from node A to node B.

It is also worth noting that it is possible to search for larger cycles (that contain more than three nodes) in the networks, as larger cycles may reveal somewhat larger area of the rotor's influence.

F. Circular octapolar virtual catheter

An electrode configuration, resembling a circular octapolar catheter with inter-electrode distance of 2 mm, was also tested. Such virtual catheter was placed in three distinct regions: i) left atrium posterior wall, where the wave propagation was flat; ii) tip of the rotor located between left PVs and left atrial appendage; and iii) focal point in the right atrium, close to the coronary sinus. Delunay triangulation was not used and the four nearest electrodes were taken as neighbors. For the three experiments, electrode positions were fixed for the entire simulation.

III. RESULTS

In the left atrium, across all 58 networks, we detected 97 cycles with three nodes. Most of these cycles occurred only in one or two networks, so they were not considered as
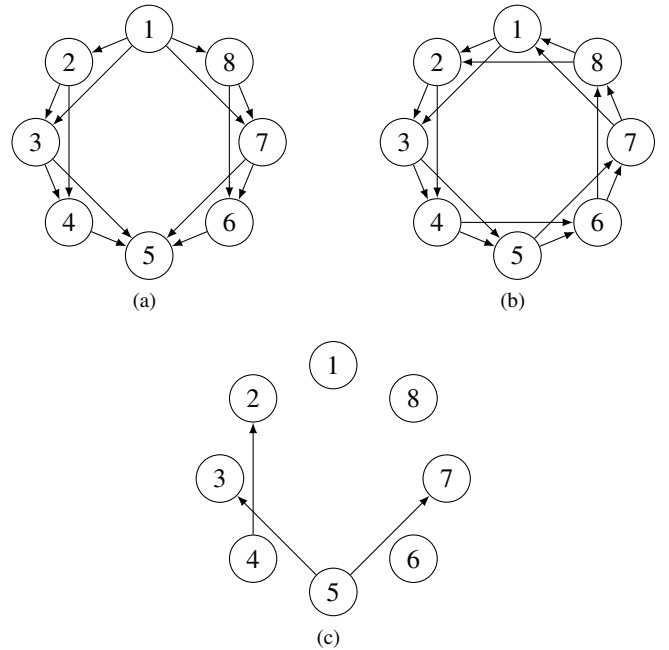

Fig. 3: Networks generated using a virtual octapolar circular catheter positioned in regions associated with: (a) a flat propagation pattern, (b) a rotor, and (c) a focal point, respectively.

candidates for the rotor location. We only considered those cycles that occurred seven or more times (900 ms or more), and they are reported in Figure 2a. The most frequent cycle occurred in 19 networks, there were two cycles that occurred 10 times, two cycles that occurred 9 times, three cycles that occurred 8 times and finally three cycles that occurred in 7 networks.

Additionally, we took into account which of these occur-

rences were in consecutive networks (Figure 2a). The longest sequence of consecutive occurrences was relatively low (less than 5 networks) in all but two cycles that occurred in 9 and 10 consecutive networks. These two cycles were considered as top candidates for the rotor location. They were positioned in the same region right next to each other, even though they did not share any common node. Interestingly, this region was the same one in which we already visually observed the existence of a rotor, looking at the electrical propagation map, produced by numerical simulations (see Figure 1a).

Figure 2b shows a portion of the result obtained by network averaging formula, focusing on the region of this rotor. The averaged network contained only two cycles with three nodes, and those two were the same ones we considered before as top candidates for the rotor location.

The results derived from the simulations involving the virtual octapolar circular electrode are ilustrated in Figure 3. Placing the virtual catheter on wavefronts with a flat propagation pattern resulted in a network with a single source node and a single sink node, where all the connections were flowing from the source to the sink. On the other hand, placing the catheter in the center of a rotor resulted in a network containing a cycle going through all the virtual electrodes of the catheter. Finally, placing the catheter in the focal point resulted in a very sparse network with just a couple of connections (the activation times are nearly identical).

IV. CONCLUSIONS

The main finding of this paper is the demonstration that a directed network can be used to represent the electrical activity in the atria during AF. We showed that directed networks can detect rotors in an *in-silico* heart model.

Network theory has had many different applications, but so far there was not a large amount of research focused on understanding AF. For example, previous studies reported the use of directed networks to identify propagation patterns during AF [13]. However, the networks in these studies were not tested for rotor detection. Directed arrows can also be created based on the concept of Granger causality between different signals [14], [15]. This approach could be an alternative way to generate the network, but it requires implementing a linear MVAR model instead of deriving the activation times. Furthermore, directed graph mapping was used to describe electrical excitation to extract the mechanism of the arrhythmia in [6], but the authors only analyzed atrial tachycardia, which is more regular than AF.

Our study presents several limitations. The 3D atrial model may be anatomically and electrophysiologically realistic, but is still simplistic in regard to wall thickness and ionic heterogeneous details [7]. We have presented simulations only for a single scenario, and patterns of real atrial waves during AF are probably more complex. The quality of the signals used is higher compared to clinical ones, which are usually contaminated by far-field effects from the ventricles and noise. Also, 400 virtual electrodes spanning the entire atrial surface may be a somewhat unrealistic scenario, so in future work, we plan to further explore the use of electrode configurations as in commercially available catheters, and sequential mapping. In addition, we leave for future works the comparison between directed network mapping and phase mapping for rotor detection.

Interestingly, network mapping may offer additional features, which can be derived from the directed graph. There already exists a large amount of algorithms in network theory, which can possibly be applied to increase our understanding of AF. For example, focal activity, which has also been described as a mechanism for AF, can likely be detected as a node in a graph which has an in-degree equal to 0 and a non-zero out-degree. We are testing this hypothesis in our on-going research.

REFERENCES

[1] P. Kirchhof, S. Benussi, D. Kotecha *et al.*, "2016 ESC Guidelines for the management of atrial fibrillation developed in collaboration with EACTS," *Eur Heart J*, vol. 37, pp. 2893–2962, 2016.

[2] H. Oral, B. P. Knight, H. Tada *et al.*, "Pulmonary Vein Isolation for Paroxysmal and Persistent Atrial Fibrillation," *Circulation*, vol. 105, pp. 1077–1081, 2002.

[3] P. Benharash, E. Buch, P. Frank *et al.*, "Quantitative Analysis of Localized Sources Identified by Focal Impulse and Rotor Modulation Mapping in Atrial Fibrillation," *Circ Arrhythm Electrophysiol*, vol. 8, pp. 554–561, 2015.

[4] S. M. Narayan, D. E. Krummen, K. Shivkumar *et al.*, "Treatment of atrial fibrillation by the ablation of localized sources: CONFIRM (Conventional Ablation for Atrial Fibrillation With or Without Focal Impulse and Rotor Modulation) Trial," *J Am Coll Cardiol*, vol. 60, no. 7, pp. 628–636, 2012.

[5] R. Vijayakumar, S. K. Vasireddi, P. S. Cuculich *et al.*, "Methodology Considerations in Phase Mapping of Human Cardiac Arrhythmias," *Circ Arrhythm Electrophysiol*, vol. 9, no. 11, 2016.

[6] N. Vandersickel, E. Van Nieuwenhuyse, N. Van Cleemput *et al.*, "Directed Networks as a Novel Way to Describe and Analyze Cardiac Excitation: Directed Graph Mapping." *Front Physiol*, vol. 10, pp. 1138–1138, 2019.

[7] A. Ferrer, R. Sebastián, D. Sánchez-Quintana *et al.*, "Detailed Anatomical and Electrophysiological Models of Human Atria and Torso for the Simulation of Atrial Activation," *PLoS One*, vol. 10, p. e0141573, 2015.

[8] M. Courtemanche, R. J. Ramirez, and S. Nattel, "Ionic mechanisms underlying human atrial action potential properties: insights from a mathematical model," *Am J Physiol Heart Circ Physiol*, vol. 275, pp. H301–H321, 1998.

[9] G. Seemann, C. Höper, F. B. Sachse *et al.*, "Heterogeneous three-dimensional anatomical and electrophysiological model of human atria," *Philos Trans A Math Phys Eng Sci*, vol. 364, pp. 1465–1481, 2006.

[10] J. Feng, L. Yue, Z. Wang, and S. Nattel, "Ionic Mechanisms of Regional Action Potential Heterogeneity in the Canine Right Atrium," *Circ Res*, vol. 83, pp. 541–551, 1998.

[11] E. A. Heidenreich, J. M. Ferrero, M. Doblaré, and J. F. Rodríguez, "Adaptive Macro Finite Elements for the Numerical Solution of Monodomain Equations in Cardiac Electrophysiology," *Ann Biomed Eng*, vol. 38, pp. 2331–2345, 2010.

[12] G. W. Botteron and J. M. Smith, "A technique for measurement of the extent of spatial organization of atrial activation during atrial fibrillation in the intact human heart," *IEEE Trans Biomed Eng*, vol. 42, pp. 579–586, 1995.

[13] U. Richter, L. Faes, F. Ravelli, and L. Sörnmo, "Propagation Pattern Analysis During Atrial Fibrillation Based on Sparse Modeling," *IEEE Trans Biomed Eng*, vol. 59, pp. 1319–1328, 2012.

[14] A. Alcaine, M. Masè, A. Cristoforetti *et al.*, "A Multi-Variate Predictability Framework to Assess Invasive Cardiac Activity and Interactions During Atrial Fibrillation," *IEEE Trans Biomed Eng*, vol. 64, pp. 1157–1168, 2017.

[15] D. Luengo, G. Ríos-Muñoz, V. Elvira *et al.*, "Hierarchical Algorithms for Causality Retrieval in Atrial Fibrillation Intracavitary Electrograms," *IEEE J Biomed Health Inform*, vol. 23, pp. 143–155, 2019.